Adsorption of typical endocrine disrupting chemicals by wheat straw biochars and the effects of the steric structure

Fang Wang[a], Qiang Zeng[a], Zhixuan Jia[a], Lei Hou[b,*], Zhong-Liang Wang[a]

[a]*Tianjin Key Laboratory of Water Resources and Environment, Tianjin Normal University, Tianjin 300387, China,
emails: wangfang@tjnu.edu.cn (F. Wang), 454515360@qq.com (Q. Zeng), 1062789148@qq.com (Z. Jia),
wangzhongliang@vip.skleg.cn (Z.-L. Wang)*
[b]*College of Ecology and Environment, Southwest Forestry University, Kunming 650224, China,
emails: houlei_1985@126.com/leihou@swfu.edu.cn*

ABSTRACT

The main objective of this study was to understand the mechanisms controlling the adsorption of endocrine-disrupting chemicals (EDCs) to biochars. The biochars were prepared by wheat straw under different pyrolysis conditions. The properties of biochars were characterized by X-ray photoelectron spectroscopy, elemental analyzer and Fourier transform infrared spectroscopy. Bisphenol A (BPA) and 17α-ethinylestradiol (EE2) were selected as the model EDCs, and phenanthrene (Phen) was chosen as the comparison chemical. Batch adsorption experiments were performed to obtain the adsorption isotherms. The results showed that the adsorption capacity of typical EDCs and Phen on biochars was as the following order: BC700 > BC500 > BC300. The adsorption affinity was significantly affected not only by the properties of biochars but also by the properties of EDCs. For Phen and EE2, which have the planar structure and bigger size, they could block the micropores of biochars, thus, the hydrophobic effect was the main adsorption mechanism. For BPA, which has the butterfly structure, it could enter into the pores of biochars and be adsorbed by the high energy sorption sites, thus, the pore-filling effect may play a key role. Meanwhile, π–π electron donor–acceptor interaction and H-bonding also play an important role in the adsorption process. These results implied that the properties of EDCs, especially their steric structure, would significantly affect their adsorption behaviors on biochars.

Keywords: Endocrine disrupting chemicals (EDCs); Adsorption mechanisms; Biochars; Steric structure

1. Introduction

Environmental estrogens are endocrine-disrupting chemicals (EDCs) that could affect the reproductive development of wildlife in the aquatic environment. They could threaten the balance of the ecological environment and human health even at very low concentrations [1–6]. In the last few decades, the removal of EDCs in the aquatic environment has raised more concerns. A kind of efficient, environmentally friendly and low-cost removal method needs to be developed [7–10].

Biochars are a kind of carbon black from pyrolysis of biomass, which showed large surface area, abundant porous structure, high aromaticity and surface heterogeneity [11]. Numerous studies have reported that biochars showed remarkable adsorption affinity for organic pollutants [12–16]. Up to now, most of the studies focused on the different physicochemical properties of biochars [13–16]. For example, Chen et al. [14] reported that with the pyrolytic temperature increased, the aromaticity of biochars increased, and the adsorption mechanisms of naphthalene,

* Corresponding author.

nitrobenzene, and n-dinitrobenzene to biochars were evolved from partition-dominant to adsorption-dominant. Sun et al. [15] reported that hydrothermal biochars consisted of more amorphous aliphatic-C compared to thermal biochars, and this could be responsible for their high sorption capacity of phenanthrene (Phen). However, besides the physicochemical properties of biochars, the different properties of the organic chemicals, especially the steric structure, were also the important factors controlling the adsorption behaviors Pan et al. [17] reported that the adsorption capacity of bisphenol A (BPA) was higher than that of 17α-ethinylestradiol (EE2) on carbon nano-materials, and this is likely because helical (diagonal) coverage of BPA on the carbon nano-materials surface and wedging of BPA into the groove and interstitial region of carbon nano-materials bundles or aggregates. Thus, not only the chemical size but also the steric structure could influence the adsorption behavior. However, there are few studies focused on the effects of different structure of EDCs on the adsorption behavior to biochars. Thus, it is of great importance to further understand the related adsorption mechanisms.

The objective of this paper was to study the adsorption behavior of typical EDCs to wheat straw biochars. BPA and EE2 were selected as the model EDCs, and Phen was chosen as the comparison chemical. The effects of the properties of biochars were discussed. The effects of hydrophobicity and steric structure of EDCs on biochar adsorption were examined, and the mechanisms were also systematically analyzed. The results of this paper could provide useful information for removing EDCs from aqueous environments.

2. Materials and methods

2.1. Materials

Phen (98%), BPA (97%) and EE2 (98%) were purchased from Sigma-Aldrich (St. Louis, MO, USA). Their physico-chemical properties and dimension information are shown in Table 1. The stock solutions of the compounds were prepared by dissolving the respective compound in methanol, and the stock solutions were stored at –20°C. The inorganic salt, sodium chloride (NaCl), was obtained from VICTOR Co. (Tianjin, China).
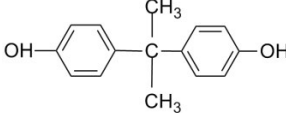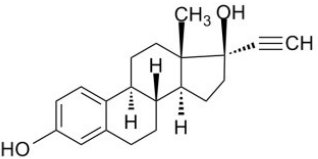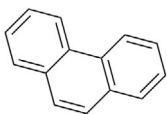
2.2. Preparation of biochars

The wheat straw was collected from North China Plain as biomass materials. The air-dried wheat straw was placed in a ceramic pot and pyrolyzed under the oxygen-limited conditions for 2 h at 300°C, 500°C and 700°C, respectively. After that, the samples were ground and passed through 0.147 mm sieve. The biochar samples were referred to BC300, BC500 and BC700, respectively, where the suffix X (X = 300, 500, 700) to BC represented the pyrolysis temperatures.

2.3. Characterization of biochars

The surface area of biochars was obtained from nitrogen adsorption–desorption isotherms using a multipoint Brunauer–Emmett–Teller (BET) method with relative pressure P/P_0 ranging from 10^{-7} to 1. The total pore volume and average pore size of samples were calculated from the desorption isotherms employing the Barrett−Joyner−Halenda (BJH) and Horvath–Kawazoe (HK) model, respectively. The element contents of the biochars were measured by X-ray photoelectron spectroscopy (XPS) (MultiLab 2000, Thermo Electron Corp., UK) and elemental analyzer (Euro EA 3000, Leeman Labs Inc., US). The point of zero charge values (pH_{PZC}) was determined by pH-drift, and the zeta potentials were determined by ZetaPALS (Brookhaven Instruments, Holtsville, NY). Fourier transform infrared spectroscopy (FTIR) (TENSOR 27, Bruker Optics Inc., Germany) was used to identify the functional groups of biochars.

Table 1
Physicochemical properties of bisphenol A (BPA), 17α-ethynylestradiol (EE2), and phenanthrene (Phen)

Adsorbate	C_{sat} (mg/L)	log K_{OW}	K_{HW}	pK_a	Molecular structure
bisphenol A[a]	380	2.2	0.27	9.6	
17α-ethynylestradiol[a]	7.6	4.2	9.55	10.4	
phenanthrene[b]	1.12	4.57	55,000	–	

[a]from Pan et al. [17].
[b]from Zhu and Pignatello [18].

2.4. Adsorption experiment

All sorption isotherms were obtained using a batch experiment modified from Nguyen et al. [19]. Certain amounts of biochar samples were added to a series of amber glass 40 mL vials with 0.01 M NaCl background solutions. The pH was adjusted to 6.0 ± 0.1 using 0.1 M NaOH or 0.1 M HCl solution. The initial concentrations of EDCs were set in a range of 0.5–30 mg L^{-1} for BPA, 0.5–15 mg L^{-1} for EE2, and 1.25–15 mg L^{-1} for Phen, respectively. The vials were placed on a rotating shaker and agitated in the dark at 8.1 rpm for 14 d. After reaching the sorption equilibrium, the vials were centrifuged for 15 min at 3,000 rpm, and then the equilibrium concentrations of EDCs in the supernatant were analyzed. The final pH of the supernatant was measured, which showed that the pH values of the solution during the adsorption process were unchanged. Each adsorption point was run in duplicates and all the vials were sealed with Teflon lined screw caps to prevent loss of the organic chemicals.

The effects of pH on the adsorption of EDCs to BC300 were also conducted using the same procedure as aforementioned. The only difference was that the initial pH values of the background solutions were set from 3.0 to 11.0 with 1.0 pH unit interval and the experiment was conducted in triplicates.

2.5. Analytical methods

The aqueous concentrations of EDCs in the supernatant were analyzed by HPLC (Agilent, HP1200, USA) equipped with a reversed-phase C18 column (5 μm × 4.6 mm × 250 mm). The concentrations of BPA, EE2 and Phen were analyzed with a fluorescence detector at 220 nm/350 nm, 206 nm/310 nm and 250 nm/330 nm, respectively. For BPA and EE2, the mobile phase was methanol and 10% acetic acid-water solution mixed in a ratio of 70:30 (v:v). For Phen, the mobile phase was methanol and water mixed in a ratio of 88:12 (v:v). The flow rate was 1 mL min^{-1}. Calibration curves contained at least 7 standards over the examined concentration range. The adsorbed mass of EDCs was calculated by mass balance.

2.6. Modeling methods

The adsorption isotherms were fitted with the Freundlich model and Dubinin-Astakhov model [20].

Freundlich model (FM):

$$q = K_F \times C_W^n \tag{1}$$

where K_F (mmol^{1-n}L^n/kg) is the adsorption affinity related parameter. n is the nonlinear coefficient. q (mmol/kg) and C_W (mmol/L) are the equilibrium solid and liquid phase concentrations, respectively.

Dubin-Astakhov model (DAM):

$$\log q_e = \log Q^0 + \left(\frac{\theta}{E}\right)^b \tag{2}$$

$$\theta = -RT\ln\left(\frac{C_e}{C_s}\right) \tag{3}$$

where Q^0 (mmol/kg) is the adsorption capacity. θ (kJ mol^{-1}) is the adsorption potential. R (8.314 × 10^{-3} kJ/(mol K)) is the universal gas constant and T (K, 273.15 + t°C) is the absolute temperature. C_s (mg L^{-1}) is the water solubility of the adsorbate. E (kJ mol^{-1}) is adsorption energy and b represents the interaction force coefficient between adsorbate and adsorbent, respectively.

3. Results and discussions

3.1. Characteristics of biochars

The element contents of different biochars were listed in Table 2. The C content of the biochar increased with the increasing pyrolysis temperature, while that of H, O and N decreased. This trend might be due to dehydration, decarboxylation, and decarbonylation effect during the pyrolysis process [21]. As shown in Table 2, the (N + O)/C ratio decreased from 28.91% to 17.38% with the increasing pyrolysis temperature, and O/C ratio decreased from 25.42% to 14.88%. This indicated that the oxygen functional groups were destroyed and disappeared at higher pyrolysis temperatures [22]. The degree of carbonization and aromaticity could be presented by the H/C ratio. The H/C ratio of BC700 was 0.02%, while that of BC300 and BC500 was much higher (1.34% for BC500 and 3.01% for BC300). This suggested that the biochars prepared at lower temperatures contained a large amount of original organic residues, such as polymeric CH$_2$, fatty acid, and some cellulose [14], and the biochar prepared at higher pyrolysis temperature was highly carbonized and exhibited a highly aromatic structure.

FTIR spectra are shown in Fig. 1. The adsorption peak at 3,392 cm^{-1} corresponded to the stretching vibration of the

Table 2
Elemental compositions and atomic ratios of the biochars prepared under different pyrolysis temperatures

Samples	Composition wt.%				Atomic ratio%		
	C	H	O	N	H/C[a]	O/C[b]	(N + O)/C[c]
BC300	60.39	1.82	15.35	2.11	3.01	25.42	28.91
BC500	61.9	0.83	13.01	1.75	1.34	21.02	23.84
BC700	62.55	0.01	9.31	1.56	0.02	14.88	17.38

[a]Atomic ratio of hydrogen to carbon.
[b]Atomic ratio of oxygen to carbon.
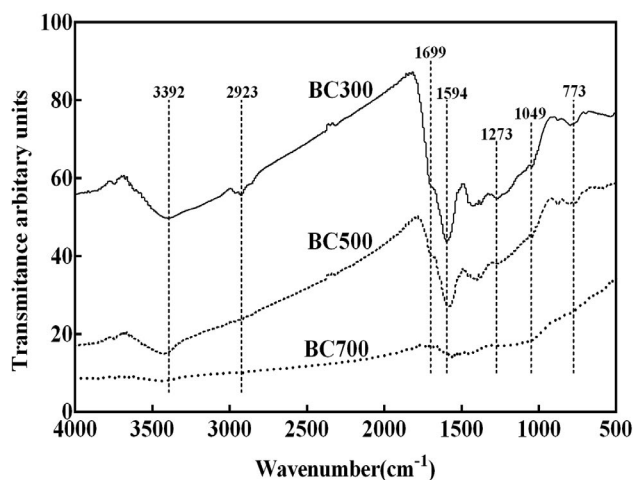[c]Atomic ratio of sum of nitrogen and oxygen to carbon.

Fig. 1. FTIR spectra of the biochars (BC300, BC500 and BC700).

–OH group, which could be attributed to the carbohydrates in the organics [23], and the peak at 1,594 cm^{-1} indicated the carbonyl stretching vibration of –COOH group [24]. Both of these two peaks decreased with the increasing pyrolysis temperature. To further identify the influence of pyrolysis temperature on the properties of biochars, the oxygen functionalities on the surface of the biochars were analyzed by XPS (Table 1 and Fig. 2). The spectrum of C1s contained four signals, including 284.6, 285.8, 287.2, and 288.8 eV, which represented C–C/C=C, C–O, C=O and COOH functional group, respectively [25] (Fig. 2). The amounts of oxygen functional groups of biochars decreased obviously with the increasing pyrolysis temperature, whereas that of C–C/C=C increased (Table 3). The point of zero charge (pH$_{PZC}$) of biochars was also tested. The pH$_{PZC}$ values of BC300, BC500 and BC700 were 10.20, 9.93 and 7.34, respectively (Table 4). The results indicated that the surface charges of biochars were negative, and the zeta potentials of biochars became more negative with the decreasing pyrolysis temperature, which was consistent with the results of zeta potential determination (Table 4). This is likely because there were more amounts of oxygen-containing functional groups (e.g. –COOH and OH) on the biochars prepared at lower pyrolysis temperature [22].

The characterization results of surface area, total pore volume, and pore size of these biochar samples are listed in Table 4. The surface area of the biochars was increased from 0.9 to 380 m^2 g^{-1} with the increasing pyrolysis temperature, and the total pore volume of the biochars showed a similar trend. Whereas the average pore size was decreased from 25.4 to 2.32 nm with the increasing pyrolysis temperature. This might because during the pyrolysis of the biomass, it decomposed and a large number of fiber chain structures were destroyed. Some substances under their volatilization temperature would deposit on the surface of the biochar and form an irregular block stack. When the pyrolysis temperature increased, the graphitic carbon was shrunk to crystalline carbon and formed micropore structures, furthermore, the aliphatic and volatile organic compounds were also burned to release more micropores and the surface area increased.
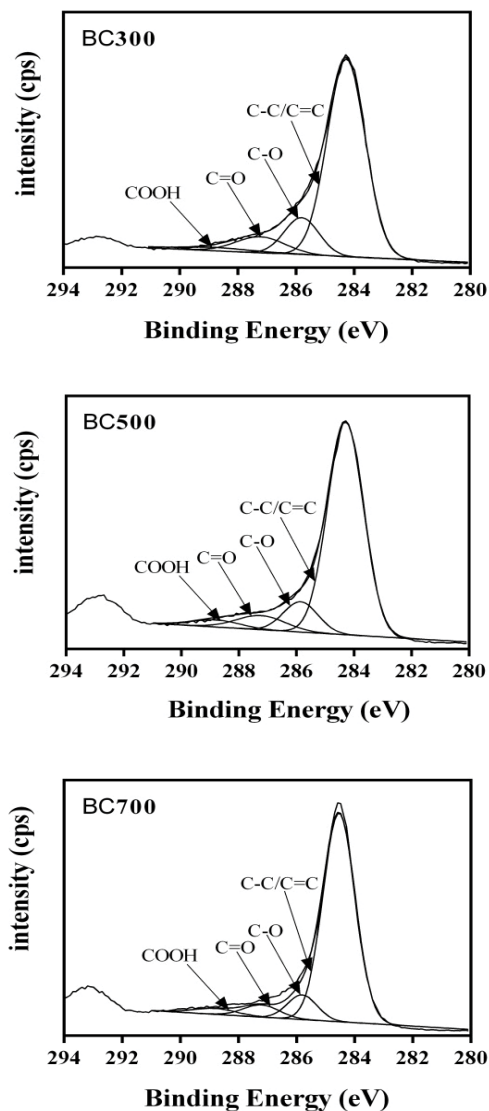

Fig. 2. XPS analysis of C1s binding energy and corresponding carbon bonds of the surface on BC300, BC500 and BC700, respectively.

3.2. Adsorption of BPA, EE2 and Phen to biochars

The sorption isotherms of Phen, BPA and EE2 were well fitted with both FM and DAM. The R^2 of the two models were all above 0.949, and the fitting parameters are summarized in Table 5. The adsorption capacity of Phen, BPA and EE2 onto biochars was increased with the increasing pyrolysis temperature, which was presented as BC700 > BC500 > BC300 (Fig. 3), indicating that adsorption efficiency might be enhanced by the increasing pyrolysis temperature, which was consistent with the previous studies [14,15,26,27]. Chen et al. [14] reported that with the increase of the pyrolytic temperature, the adsorption affinities of naphthalene, nitrobenzene, and n-dinitrobenzene to biochars were enhanced. Sun et al. [15] also found similar results.

The nonlinearity of sorption isotherms indicates the heterogeneous distribution of adsorption sites of the

Table 3
Types and content ratios of functional groups on the surface of biochars

Functional groups[a]	Binding energy (eV)[b]	Atomic percentage (%)[c]		
		BC300	BC500	BC700
C–C/C=C	284.3	75.45	78.67	82.72
C–O	285.8	12.79	10.68	8.88
C=O	287.2	7.96	7.10	5.34
COOH	288.8	3.80	3.56	3.06

[a,b]Distribution of carbon species was determined from the C1s spectra of X-ray photoelectron spectroscopy.
[c]Calculated from the analysis of C1s spectra.

adsorbents [28]. The sorption isotherms of Phen, BPA and EE2 were nonlinear, and the degree of the nonlinearity was increased with the increasing of pyrolysis temperature, indicating by the decreased n values of the Freundlich sorption model (Table 5). Due to the more aliphatic structure and loose texture of the biochars prepared at low pyrolysis temperature, the rubbery region was formed. Phen, BPA and EE2 molecules could dissolve in the rubbery region by partition effect. However, with the increasing of pyrolysis temperature, the dense aromatic ring structure of biochars was formed, which caused the decrease of the rubbery region, and the sorption nonlinearity was enhanced exhibited smaller values of n parameters [29]. Thus, the partition effect may not be the main effect controlling the adsorption on

Table 4
Specific surface area, total pore volume, pore size, ζ potential and pH$_{PZC}$ of the biochars prepared under different temperatures

Samples	Specific surface area[a] (m^2/g)	Pore volume[a] (cm^3/g)	Pore size[a] (nm)	ζ potential[b] (mV)	pH$_{PZC}$[c]
BC300	0.90	0.0057	25.4	−11.0	10.2
BC500	58	0.053	3.66	−37.1	9.93
BC700	380	0.22	2.32	−40.7	7.34

[a]Calculated by the BET-N$_2$ method.
[b]Determined by ZetaPALS.
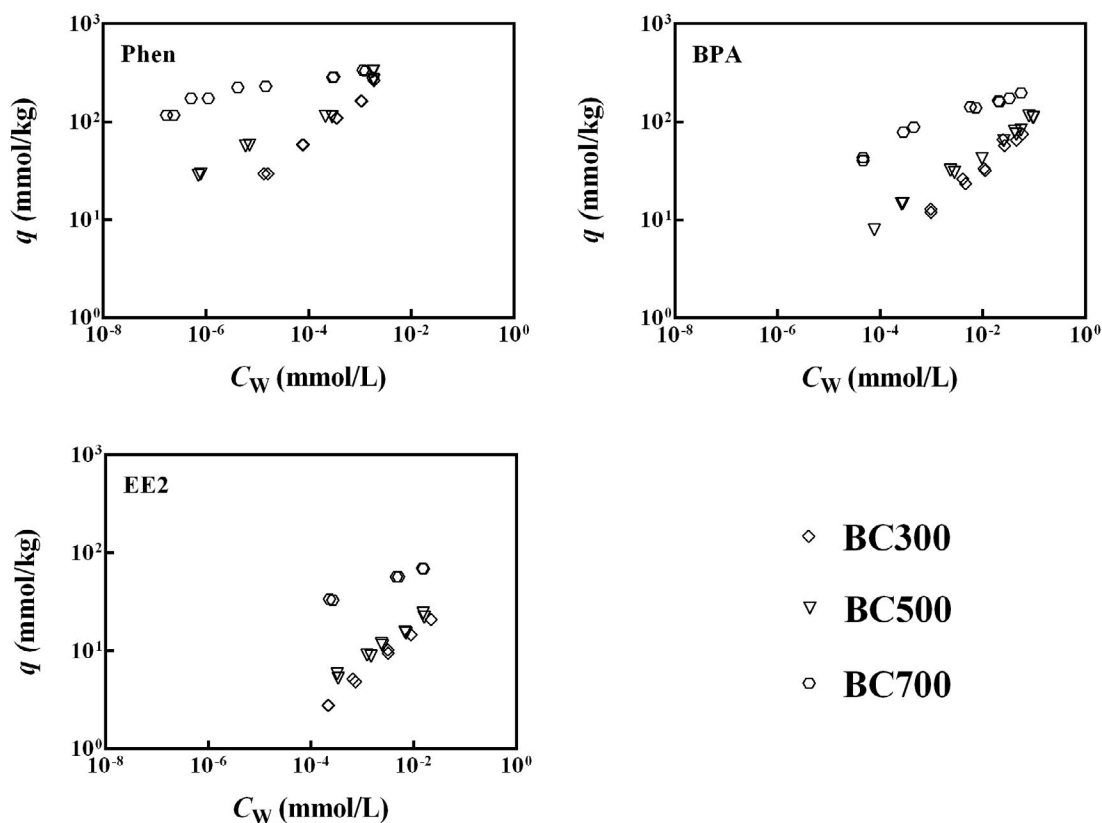[c]Determined by pH-drift.

Fig. 3. Comparison of the actual sorption onto biochars (BC300, BC500 and BC700) with the pollutant of Phen, BPA and EE2, respectively.

Table 5
Results of fitting parameters and correlation coefficients for the adsorption isotherms of BPA, EE2 and Phen to biochars by Freundlich and Dubin-Astakhov models

Adsorbate	Adsorbent	FM[a]			DAM[b]				$\log K_d{}^d$	$(\log K_d)'$	
		K_F (mmol^{1-n}L^n/kg)^c	n	R^2	$Q°$ (mmol/kg)	E (kJ/mol)	b	R^2		$C_W = 0.01C_{sat}$	$C_W = 0.001C_{sat}$
BPA	BC300	260 ± 40	0.44 ± 0.04	0.951	160 ± 60	13.6 ± 1.4	1.3 ± 0.5	0.964	3.11–4.12	3.49	3.96
	BC500	280 ± 30	0.38 ± 0.03	0.981	200 ± 50	16.4 ± 1.9	0.9 ± 0.2	0.990	3.06–5.01	3.84	4.45
	BC700	320 ± 10	0.17 ± 0.01	0.980	280 ± 50	29.3 ± 1.8	1.2 ± 0.3	0.978	2.38–4.80	4.56	5.46
EE2	BC300	100 ± 10	0.41 ± 0.01	0.996	60 ± 30	14.8 ± 3.0	1.2 ± 0.5	0.979	2.98–4.11	3.42	4.01
	BC500	110 ± 20	0.38 ± 0.02	0.975	80 ± 70	15.2 ± 6.5	1.0 ± 0.6	0.986	3.14–4.25	3.53	4.15
	BC700	150 ± 10	0.18 ± 0.01	0.998	90 ± 10	29.4 ± 1.2	1.7 ± 0.3	0.994	3.59–5.16	4.15	4.97
Phen	BC300	7,100 ± 2,700	0.53 ± 0.06	0.961	480 ± 120	12.2 ± 1.6	0.8 ± 0.1	0.996	5.15–6.34	6.20	6.76
	BC500	3,300 ± 1,300	0.39 ± 0.06	0.951	390 ± 240	21.1 ± 8.2	0.6 ± 0.3	0.974	5.16–7.60	6.12	6.74
	BC700	650 ± 50	0.10 ± 0.01	0.949	330 ± 20	41.8 ± 5.5	1.9 ± 0.5	0.964	5.41–8.70	6.30	7.13

[a]FM: Freundlich model.
[b]DAM: Dubin-Astakhov model.
[c]Values after ± sign indicate relative standard deviation.
[d]Sorption distribution coefficient with units of (L/kg), C_{sat} is the water solubility of BPA (380 mg/L) EE2 (7.6 mg/L) or Phen (1.12 mg/L).

biochars, especially for the biochars prepared at high pyrolysis temperature.

To further understand the mechanisms of EDCs adsorption to biochars, the adsorption isotherms of different compounds to the same biochars were compared. As shown in Fig. 4, the adsorption capacity of Phen, BPA and EE2 onto the biochar under the same pyrolysis temperature was following the order: Phen > BPA > EE2. The adsorption energy (E) was calculated by the DAM model and shown in Table 5. The E values of Phen, BPA and EE2 onto biochars were increased with the increasing pyrolysis temperature (Table 5), which indicated the adsorption energy (E) was stronger when the pyrolysis temperature was higher. It was reported that there are a lot of hydrophobic sites on the surface of biochars, thus, the hydrophobic interaction was one of the main mechanisms in hydrophobic organic compounds adsorption to biochars [30,31]. Wang et al. [32] had found that the hydrophobic interaction was the main adsorption mechanism of large aperture absorbent for 1-naphthol, 1-naphthylamine and Phen, which had a similar structure but different hydrophobicity. In our study, the hydrophobicity of Phen was higher than BPA and EE2 (supported by C_{sat} and log K_{OW} values in Table 1). Thus, hydrophobic interaction was the main reason that Phen showed the strongest adsorption affinity on the biochars.

It is noted that the adsorption affinity of BPA on biochars was stronger than that of EE2, although the hydrophobicity of BPA was weaker than EE2. This indicated that other mechanisms are controlling the adsorption behavior besides the hydrophobic effect. To further explore the adsorption mechanisms that eliminated the hydrophobic effect, n-hexadecane was used as a reference solvent to normalize the adsorption isotherms [30]. The equation of normalization of n-hexadecane is $C_H = C_W \cdot C_{HW}$, where C_H represents the normalized concentrations of organic pollutants in the n-hexadecane after partition equilibrium; C_W is the equilibrium aqueous phase concentrations of organic pollutants; C_{HW} is the n-hexadecane distribution coefficients of organic pollutants [30]. The comparison results of the normalized sorption isotherms of Phen, BPA and EE2 are shown in Fig. 5. The adsorption trends were presented as BPA > Phen > EE2. This is likely because of the unique structure of BPA compared with the planar structure of Phen and EE2. The molecule of BPA has a butterfly structure, and the C–C bond connected with both sides of the phenol hydroxyl of BPA could be rotated freely [15,17]. This could not only reduce the size of the three-dimensional space of BPA but also make the molecules of BPA easier to enter the micropores of the biochars, of which the mean size was much bigger than that of BPA (Table 4). However, Phen and EE2 both had a planar structure. They might block the micropores and could not go inside the pore adsorption sites as shown in Fig. 7. Thus, pore-filling/blockage was another important mechanism in EDCs adsorption to biochars. On the other hand, the abundant benzene rings of the biochars make biochars could be either a π-electron donor or π-electron acceptor. BPA had two benzene rings and two hydroxyl substituents on the benzene ring, which were strong electron donor groups. Thus, BPA could act as a strong π-electron donor. Therefore, the π–π electron donor–acceptor (EDA) interactions were stronger than EE2 and Phen. The previous studies have shown that π–π EDA interaction between the
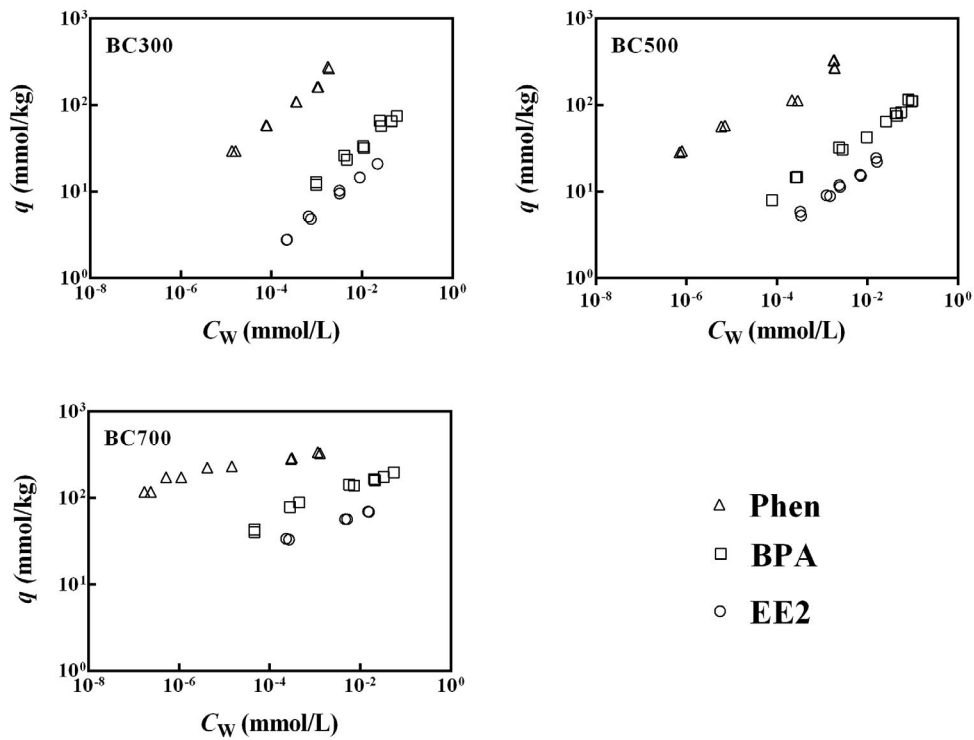
Fig. 4. Adsorption isotherm of Phen, BPA and EE2 by biochars. q (mmol/kg) and C_W (mmol/L) are equilibrium concentrations of Phen, BPA and EE2 on biochars (BC300, BC500 and BC700) and in aqueous solution, respectively.
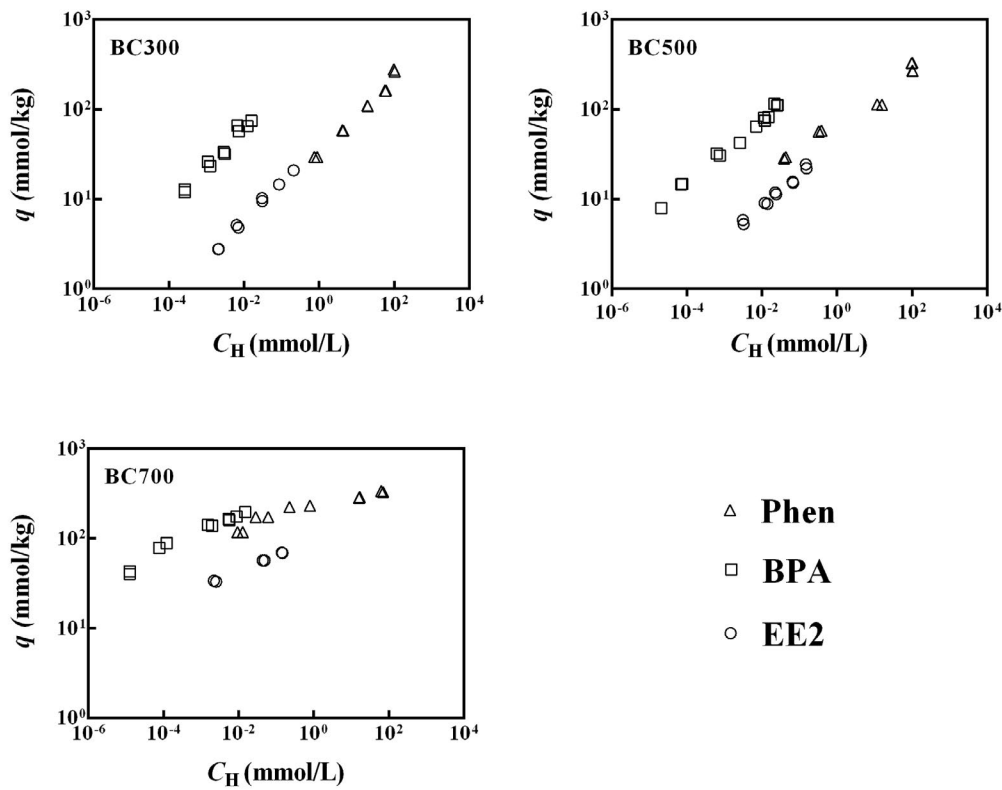

Fig. 5. Adsorption isotherms of different adsorbates to biochars (BC300, BC500 and BC700). Adsorption data are normalized by the hydrophobic effect using *n*-hexadecane as the reference solvent.

electron donor that was rich in π-electron and the highly polarized π-electron acceptor on the surfaces of biochars, was the mainly enhanced mechanism rather than hydrophobic interaction and van der Waals forces [15,17]. Sun et al. [15] also reported that the π–π EDA interaction between BPA and biochars was stronger than that between EE2 and biochars. Furthermore, the hydrogen bond between BPA and the O-containing groups on the surface of biochars was stronger than that between EE2 and biochars, because BPA is more polar than EE2. This could also explain the higher adsorption of BPA compared to EE2. Thus, the H-bonding may also play an important role in the adsorption process.

Interestingly, with the pyrolysis temperature increased, the gap between BPA and the other two compounds became smaller, especially for Phen. This is likely because the hydrophobicity of biochar increased with the increase of pyrolysis temperature, and the contribution of the hydrophobic effect between EDCs and biochars increased, especially for the most hydrophobic compound (Phen).

The effect of pH on the adsorption behaviors of Phen, BPA and EE2 on BC300, which contained the highest O-functional groups, were also examined as shown in Fig. 6. The adsorption efficiency of Phen, BPA and EE2 were not significantly affected by pH, although the change of pH values could influence the protonation-deprotonation surface O-functional groups of biochars.

3.3. Adsorption mechanisms of EDCs to biochars

To better understand the mechanisms controlling the adsorption of EDCs to biochars, the schematic diagram of adsorption mechanisms are summarized in Fig. 7. Many mechanisms controlled the adsorption behaviors of EDCs to biochars, whereas the dominant mechanism was depended on the characteristics of both EDCs and biochars. When the pyrolysis temperature was low, the composition of biochar was more aliphatic and loose with a large amount of rubbery regions, and the partition effect could be an important mechanism. And for BPA and EE2, H-bonding might also play a role as the abundant –OH groups on the surface of biochar. With the increase of pyrolysis temperature, the
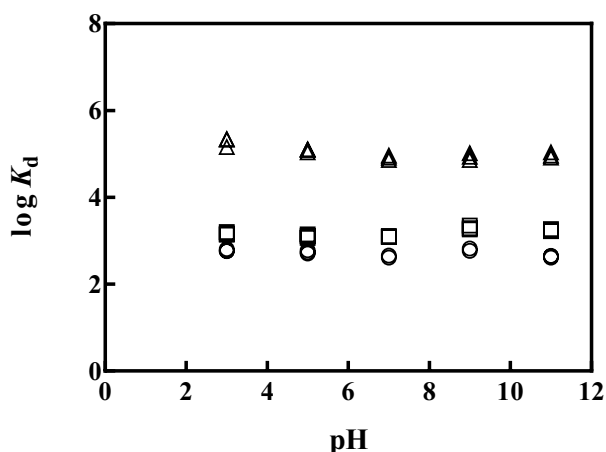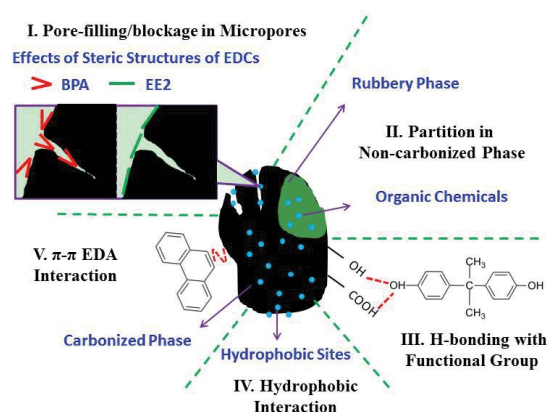

Fig. 7. Schematic diagram of adsorption mechanisms of EDCs to biochars.

organic matter in biochar would be burned or degraded along with the decrease of oxygen amounts, and the partition and H-bonding effect might be weakened. However, the disappearance of organic matter would increase the aromaticity and hydrophobicity of the biochar, and micropores were also developed or released, thus, other mechanisms started to play the important roles, such as hydrophobic interaction, π–π EDA interactions, pore-filling/blockage, etc. All of these mechanisms were highly related to the properties of EDCs: (1) hydrophobic interaction was more important for Phen, the most hydrophobic chemicals in this research; (2) π–π EDA interactions and H-bonding might work for BPA and EE2, especially for BPA as the electron-withdrawing effect of the two hydroxyl groups on the benzene rings; and (3) pore-filling mechanism was most important mechanisms, especially for the butterfly structure compound (BPA).

3.4. Environmental significance of this work

There is plenty of wheat straws produced in China every year, a part of which could be collected and prepared into biochars, thus the low-cost preparation of these excellent sorbents for EDCs could be guaranteed. Based on our research results, EDCs with different structures would have different adsorption affinities on biochars due to diverse adsorption mechanisms, and structural properties of biochars (e.g. pore volume and micropore structures, etc.) might play the dominant role. After we fully understand the relationship between the adsorption affinity of EDCs to biochars and their structural characteristics, we could prepare biochars with different structural characteristics according to the types of EDCs, and make the biochars more efficient in the removal of EDCs and wastewater treatment.

4. Conclusion

The physicochemical properties of biochars were greatly influenced by pyrolysis temperature. Higher pyrolysis temperature could reduce the amounts of polarity groups and also increase the aromaticity of biochars. Large surface area

Fig. 6. Adsorption of Phen (△), BPA (□) and EE2 (○) onto BC300 at various pH conditions.

and more micropore structures of biochars could be developed when pyrolysis temperature was high. The adsorption affinity of EDCs was increased with the increasing pyrolysis temperature, and the adsorption affinity of Phen, BPA and EE2 onto the same biochars was following the order that Phen > BPA > EE2. The main adsorption mechanisms of EDCs onto the biochars were significantly determined by the properties of biochars and EDCs. For the compound with a butterfly structure, BPA, pore-filling effect was the most important mechanism. For the planar and hydrophobic compounds, EE2 and Phen, hydrophobic effect played a key role. These results could help us develop efficient and inexpensive adsorbents special for different compounds with different structures and properties in wastewater treatment.

Acknowledgments

References

[1] O. Lee, A. Takesono, M. Tada, C.R. Tyler, T. Kudoh, Biosensor zebrafish provide new insights intopotential health effects of environmental estrogens, Environ. Health Perspect., 120 (2012) 990–996.

[2] S. Jobling, R. Williams, A. Johnson, A. Taylor, M.G. Sorokin, M. Nolan, C.R. Tyler, R.V. Aerle, E. Santos, G. Brighty, Predicted exposures to steroid estrogens in UK rivers correlate with widespread sexual disruption in wild fish populations, Environ. Health Perspect., 114 (2006) 32–39.

[3] Z.H. Liu, G.N. Lu, H. Yin, Z. Dang, B. Rittmann, Removal of natural estrogens and their conjugates in municipal wastewater treatment plants: a critical review, Environ. Sci. Technol., 49 (2015) 5288–5300.

[4] J.Y. Hu, T. Aizawa, S. Ookubo, Products of aqueous chlorination of bisphenol A and their estrogenic activity, Environ. Sci. Technol., 36 (2002) 1980–1987.

[5] B.M. Armstrong, J.M. Lazorchak, K.M. Jensen, H.J. Haring, M.E. Smith, R.W. Flick, D.C. Bencic, A.D. Biales, Reproductive effects in fathead minnows (*Pimphales promelas*) following a 21 d exposure to 17α-ethinylestradiol, Chemosphere, 144 (2016) 366–373.

[6] P.H. Chou, Y.L. Lin, T.C. Liu, K.Y. Chen, Exploring potential contributors to endocrine disrupting activities in Taiwan's surface waters using yeast assays and chemical analysis, Chemosphere, 138 (2015) 814–820.

[7] L. Zhou, R. Liu, A. Wilding, A. Hibberd, Sorption of selected endocrine disrupting chemicals to different aquatic colloids, Environ. Sci. Technol., 41 (2007) 206–213.

[8] O. Braga, G.A. Smythe, A.I. Schäfer, A.J. Feitz, Fate of steroid estrogens in Australian inland and coastal wastewater treatment plants, Environ. Sci. Technol., 39 (2005) 3351–3358.

[9] E.J. Rosenfeldt, K.G. Linden, Degradation of endocrine disrupting chemicals bisphenol A, ethinyl estradiol, and estradiol during UV photolysis and advanced oxidation processes, Environ. Sci. Technol., 38 (2004) 5476–5483.

[10] R.A. Torres, C. Pétrier, E. Combet, F. Moulet, C. Pulgarin, Bisphenol A mineralization by integrated ultrasound-UV-iron (II) treatment, Environ. Sci. Technol., 41 (2007) 297–302.

[11] E. Kim, C. Jung, J. Han, N. Her, C.M. Park, M. Jang, A. Son, Y. Yoond, Sorptive removal of selected emerging contaminants using biochar in aqueous solution, J. Ind. Eng. Chem., 36 (2016) 364–371.

[12] M. Kołtowski, I. Hilber, T.D. Bucheli, P. Oleszczuk, Effect of activated carbon and biochars on the bioavailability of polycyclic aromatic hydrocarbons in different industrially contaminated soils, Environ. Sci. Pollut. Res., 23 (2016) 11058–11068.

[13] S.E. Hale, J. Lehmann, D. Rutherford, A.R. Zimmerman, R.T. Bachmann, V. Shitumbanuma, A. O'Toole, K.L. Sundqvist, H.H. Arp, G. Cornelissen, Quantifying the total and bioavailable polycyclic aromatic hydrocarbons and dioxins in biochars, Environ. Sci. Technol., 46 (2012) 2830–2838.

[14] B.L. Chen, D.D. Zhou, L.Z. Zhu, Transitional adsorption and partition of nonpolar and polar aromatic contaminants by biochars of pine needles with different pyrolytic temperatures, Environ. Sci. Technol., 42 (2008) 5137–5143.

[15] K. Sun, K. Ro. M.X. Guo, J. Novak, H. Mashayekhi, B.S. Xing, Sorption of bisphenol A, 17α-ethinyl estradiol and phenanthrene on thermally and hydrothermally produced biochars, Bioresour. Technol., 102 (2011) 5757–5763.

[16] X.F. Tan, Y.G. Liu, G.M. Zeng, X. Wang, X.J. Hu, Y.L. Gu, Z.Z. Yang, Application of biochar for the removal of pollutants from aqueous solutions, Chemosphere, 125 (2015) 70–85.

[17] B. Pan, D. Lin, H. Mashayekhi, B.S. Xing, Adsorption and hysteresis of bisphenol A and 17α-ethinyl estradiol on carbon nanomaterials, Environ. Sci. Technol., 42 (2008) 5480–5485.

[18] D.Q. Zhu, J.J. Pignatello, Characterization of aromatic compound sorptive interactions with black carbon (charcoal) assisted by graphite as a model, Environ. Sci. Technol., 39 (2005) 2033–2041.

[19] Y.K. Choi, E. Kan, Effects of pyrolysis temperature on the physicochemical properties of alfalfa-derived biochar for the adsorption of bisphenol a and sulfamethoxazole in water, Chemosphere, 218 (2018) 741–748.

[20] K. Yang, B.S. Xing, Adsorption of organic compounds by carbon nanomaterials in aqueous phase: Polanyi theory and its application, Chem. Rev., 110 (2010) 5989–6008.

[21] G.N. Kasozi, A.R. Zimmerman, P. Nkedi-Kizza, B. Gao, Catechol and humic acid sorption onto a range of laboratory-produced black carbons (biochars), Environ. Sci. Technol., 44 (2010) 6189–6195.

[22] X. Xiao, B.L. Chen, L.Z. Zhu, Transformation, morphology, and dissolution of silicon and carbon in rice straw-derived biochars under different pyrolytic temperatures, Environ. Sci. Technol., 48 (2014) 3411–3419.

[23] G. Chu, J. Zhao, F. Chen, X. Dong, D. Zhou, N. Liang, M. Wu, B. Pan, C.E.W. Steinberg, Physi-chemical and sorption properties of biochars prepared from peanut shell using thermal pyrolysis and microwave irradiation, Environ. Pollut., 227 (2017) 372–379.

[24] B.L. Chen, E.J. Johnson, B. Chefetz, L.Z. Zhu, B.S. Xing, Sorption of polar and nonpolar aromatic organic contaminants by plant cuticular materials: role of polarity and accessibility, Environ. Sci. Technol., 39 (2005) 6138–6146.

[25] F.X. Yao, M.C. Arbestain, S. Virgel, F. Blanco, J. Arostegui, J.A. Maciá-Agulló, F. Macìas, Simulated geochemical weathering of a mineral ash-rich biochar in a modified Soxhlet reactor, Chemosphere, 80 (2010) 724–732.

[26] M.X. Xie, W. Chen, Z.Y. Xu, S.R. Zheng, D.Q. Zhu, Adsorption of sulfonamides to demineralized pine wood biochars prepared under different thermochemical conditions, Environ. Pollut., 186 (2014) 187–194.

[27] P. Peng, Y.H. Lang, X.M. Wang, Adsorption behavior and mechanism of pentachlorophenol on reed biochars: pH effect, pyrolysis temperature, hydrochloric acid treatment and isotherms, Ecol. Eng., 90 (2016) 225–233.

[28] X.Y. Guo, X.L. Wang, X.Z. Zhou, X. Ding, B. Fu, S. Tao, B.S. Xing, Impact of the simulated diagenesis on sorption of naphthalene

and 1-naphthol by soil organic matter and its precursors, Environ. Sci. Technol., 47 (2013) 12148–12155.

[29] B. Pan, P. Wang, M. Wu, J. Li, D. Zhang, D. Xiao, Sorption kinetics of ofloxacin in soils and mineral particles, Environ. Pollut., 171 (2012) 185–190.

[30] F. Wang, J.H. Haftka, T.L. Sinnige, J.L. Hermens, W. Chen, Adsorption of polar, nonpolar, and substituted aromatics to colloidal graphene oxide nanoparticles, Environ. Pollut., 186 (2014) 226–233.

[31] H.B. Peng, D. Zhang, B. Pan, J.H. Peng, Contribution of hydrophobic effect to the sorption of phenanthrene, 9-phenanthrol and 9, 10-phenanthrenequinone on carbon nanotubes, Chemosphere, 168 (2017) 739–747.

[32] X.L. Wang, J.L. Lu, B.S. Xing, Sorption of organic contaminants by carbon nanotubes: influence of adsorbed organic matter, Environ. Sci. Technol., 42 (2008) 3207–3212.